

# Multilevel Monte Carlo Combined with Numerical Smoothing for Robust and Efficient Option Pricing and Density Estimation

Christian Bayer\*

Chiheb Ben Hammouda<sup>†</sup>Raúl Tempone<sup>‡§</sup>

## Abstract

The multilevel Monte Carlo (MLMC) is a highly efficient approach to estimate expectations of a functional of a solution to a stochastic differential equation. However, MLMC estimators may be unstable and have a nonoptimal complexity in case of low regularity of the observable. To overcome this issue, we extend our idea of numerical smoothing, introduced in our previous work (ArXiv abs/2111.01874 (2021)) in the context of deterministic quadrature methods, to the MLMC setting. The numerical smoothing technique is based on root finding methods combined with one-dimensional numerical integration with respect to a single well-chosen variable. Motivated by option pricing and density estimation problems, our analysis and numerical experiments show that the employed numerical smoothing significantly improves the complexity and robustness (making the kurtosis at deep levels bounded) of the MLMC method. In particular, the smoothness theorem presented in our previous work (ArXiv abs/2111.01874 (2021)) enables us to recover the MLMC complexities obtained for Lipschitz functionals. Moreover, our approach efficiently estimates density functions, a task that previous methods based on Monte Carlo or MLMC fail to achieve at least in moderate to high dimensions. Finally, our approach is generic and can be applied to solve a broad class of problems, particularly for approximating distribution functions, financial Greeks computation, and risk estimation.

**Keywords** Multilevel Monte Carlo, Numerical smoothing, Option pricing, Density estimation, Robustness, Complexity, Monte Carlo, Distribution functions, Greeks, Risk estimation

**2010 Mathematics Subject Classification** 62P05, 65C05, 65D30, 65Y20, 91G20, 91G60.

## 1 Introduction

In several applications such as digital and barrier options pricing, computation of financial Greeks, risk estimation, and estimation of distribution functions or densities one is interested in efficiently computing the expectation of a functional  $g$  of a solution,  $X$ , to a stochastic differential equation (SDE):

$$(1.1) \quad \mathbb{E} [g(X)],$$

---

\*Weierstrass Institute for Applied Analysis and Stochastics (WIAS), Berlin, Germany.

<sup>†</sup>Chair of Mathematics for Uncertainty Quantification, RWTH Aachen University, Germany (benhammouda@uq.rwth-aachen.de).

<sup>‡</sup>King Abdullah University of Science and Technology (KAUST), Computer, Electrical and Mathematical Sciences & Engineering Division (CEMSE), Saudi Arabia.

<sup>§</sup>Alexander von Humboldt Professor in Mathematics for Uncertainty Quantification, RWTH Aachen University, Germany.

even when  $g$  exhibits low regularity.

Monte Carlo (MC) methods (standard MC and multilevel Monte Carlo (MLMC) [13]) can be used to approximate the expectation in (1.1). Although the convergence rate of the standard MC is insensitive to the input space dimensionality and regularity of the observable  $g$ , the convergence is slow. On the other hand, MLMC, which is based on a hierarchical representation of the expectation of interest and has a better convergence speed than the standard MC, is negatively affected by low regularity of  $g$ . These adverse effects consist of (i) a nonoptimal variance decay rate that affects the complexity of the MLMC method (see [3, 14] and Sections 3 and 4) and (ii) a high kurtosis at the deep levels of MLMC, which deteriorates the robustness and performance of the estimator (see Sections 3 and 4). Furthermore, when estimating densities ( $g$  presented in (1.1) is a Dirac delta function), standard (without smoothing) or regularized MC and MLMC methods either fail due to the infinite variance or have an error that explodes with the dimension (see Subsection 2.3).

This work addresses the abovementioned challenges for cases where an analytic (explicit) smoothing of the integrand cannot be performed. We extend our numerical smoothing idea introduced in [4] to the MLMC estimator to improve its robustness and complexity when pricing options with discontinuous payoffs or estimating densities. This technique, which was previously introduced in [4] in the context of deterministic quadrature methods when pricing options, is based on root-finding methods combined with a one-dimensional numerical integration with respect to (w.r.t.) a single well-chosen variable.

Previously, the authors in [3, 14] used MLMC without smoothing for pricing options with discontinuous payoffs and obtained a poor performance. Afterward, different treatments [9, 22, 15, 1, 20, 17] were proposed to efficiently deal with discontinuous functionals when using MLMC. For instance, [22] used implicit smoothing based on conditional expectation tools. Although this technique improved the variance decay rate and the complexity of MLMC when using the Milstein scheme, it did not help with the Euler discretization. Furthermore, in general cases, one may have dynamics where it is difficult to derive an analytic expression for the conditional expectation of interest. Finally, using the Milstein scheme has major drawbacks: (i) it is expensive to compute for high-dimensional dynamics, (ii) the design of a good coupling strategy in the MLMC setting is challenging, and (iii) the kurtosis may explode at the deep levels. Similar observations hold for [9], where a change of measure was introduced for Milstein discretization. The authors in [15] suggested a different approach based on parametric smoothing. They carefully constructed a regularized version of the observable, based on a regularization parameter that depends on the function of interest's degree of smoothness. Despite offering better performance than the standard (without smoothing) MLMC estimator and a clear setting for theoretical analysis, this approach has a practical disadvantage regarding the difficulty of its generalization toward the cases where (i) no prior knowledge of the degree of smoothness of the function of interest exists and (ii) more challenging dynamics than the geometric Brownian motion (GBM) which was considered in [15]. The authors in [1] used Malliavin calculus integration by parts to handle discontinuous payoffs. They split the payoff function into a smooth component (treated by standard MLMC) and a compactly supported discontinuous part (treated via Malliavin MLMC).

Compared with the case without smoothing, our analysis and numerical experiments show that the employed numerical smoothing technique improves (i) the complexity of the MLMC estimator owing to the improvement of the variance decay rate and (ii) the estimator's robustness by reducing and better controlling the kurtosis at deep levels (making it bounded). In particular, we show that the smoothness theorem presented in [4] enables us to recover the MLMC complexities obtained

for smooth or Lipschitz functionals. We emphasize that using the Euler scheme, we obtain similar rates of variance decay and MLMC complexity as those reported in [11, 22] without employing higher order schemes, such as the Milstein scheme. Furthermore, we show that our approach allows us to efficiently estimate density functions: a task that previous methods based on MC or MLMC either fail to achieve due to the infinite variance, or have an error that explodes with the dimension. Notably, estimating densities using the method in [15] results in a mean square error (MSE) behavior that is similar to the behavior obtained with the kernel density techniques, where the error increases exponentially w.r.t. the dimension of the underlying process. However, thanks to the exact conditional expectation w.r.t. the Brownian bridge, the error of our approach is only restricted to the root-finding error when approximating the exact location of the discontinuity (see Section 2.3 for further details); therefore, it is insensitive to the increase of dimensions. Although we provide pointwise density estimates, our approach can be easily extended to approximate functions using ideas that are similar to those introduced in [15, 20] using interpolation grids. Finally, compared with [11, 22, 15, 17], we provide numerical results for the Heston model, which has nonsmooth diffusion coefficients and where discretization is needed, unlike the GBM dynamics, which is an instructive example herein to showcase our approach.

Finally, we emphasize that some previous studies [15, 16, 6, 5] reported the issue of high kurtosis when using the MLMC estimator for different applications. In this work, we focus on option pricing problems and density estimations tasks where high kurtosis is due to the low regularity of the observable. Herein, we show how the numerical smoothing idea enables us to overcome this undesirable feature in the estimator.

The remainder of the paper is organized as follows. In Section 2, we introduce our problem setting and explain the technique of numerical smoothing. In Subsection 2.2, we briefly revisit the idea introduced in [4]. Then in Subsection 2.3, we extend it for the density estimation application. In Section 3, we explain and analyze our approach, where we combine the MLMC estimator with numerical smoothing. We present the error, work and robustness analysis in Subsections 3.1, 3.2, and 3.3, respectively. Finally, in Section 4, we report and analyze the results of the different numerical experiments conducted for pricing digital options and density estimation under the GBM and Heston models. Further, we illustrate the advantages of our approach over to the standard MLMC estimator (without smoothing).

## 2 Problem Setting and Numerical Smoothing Idea

### 2.1 Problem setup

To showcase the application of our approach, we work mainly with two possible structures of observable  $g$ :

$$(2.1) \quad \text{(i) } g(\mathbf{x}) = \mathbf{1}_{\{\phi(\mathbf{x}) \geq 0\}}; \text{ (ii) } g(\mathbf{x}) = \delta(\phi(\mathbf{x}) = 0),^1$$

where the function  $\phi$  is assumed to be smooth.

We introduce the notation  $\mathbf{x}_{-j}$  to denote a vector with length  $d-1$ , representing all the variables other than  $x_j$  in  $\mathbf{x} \in \mathbb{R}^d$ ,  $d \geq 1$ . Abusing notation, we define  $\phi(\mathbf{x}) = \phi(x_j, \mathbf{x}_{-j})$ , and for the ease of

---

<sup>1</sup>Case (i) applies to pricing digital options or estimating distribution functions. Case (ii) applies to density estimation where  $\delta(\cdot)$  is the Dirac delta function. Both cases can be related to Greeks computation.

presentation, we assume that for fixed  $\mathbf{x}_{-j}$ , the function  $\phi(x_j, \mathbf{x}_{-j})$  has a simple root or is positive for all  $x_j \in \mathbb{R}$ . This is guaranteed by the monotonicity condition (2.2) and infinite growth condition (2.3), which are assumed for some  $j \in \{1, \dots, d\}$ .

(2.2)

$$\frac{\partial \phi}{\partial x_j}(\mathbf{x}) > 0, \forall \mathbf{x} \in \mathbb{R}^d \text{ (Monotonicity condition)}^2$$

(2.3)

$$\lim_{x_j \rightarrow +\infty} \phi(\mathbf{x}) = \lim_{x_j \rightarrow +\infty} \phi(x_j, \mathbf{x}_{-j}) = +\infty, \forall \mathbf{x}_{-j} \in \mathbb{R}^{d-1} \text{ or } \frac{\partial^2 \phi}{\partial x_j^2}(\mathbf{x}) \geq 0, \forall \mathbf{x} \in \mathbb{R}^d \text{ (Growth condition)}.$$

As stated in Remark 2.4 in [4], the numerical smoothing idea and consequently our approach presented herein can be easily extended to the case of finite numerous roots. Furthermore, we revisit this extension for the case of densities estimation in Subsection 2.3.

## 2.2 Revisiting the idea of numerical smoothing

In this Subsection, we briefly revisit the numerical smoothing idea that was introduced in [4] in the context of deterministic quadrature methods when pricing options. We refer to Subsections 2.1 and 2.2 in [4] for more related details. We aim to efficiently approximate  $\mathbb{E}[g(\mathbf{X}_T)]$  at final time  $T$ , where  $\mathbf{X}(t) := (X^{(1)}(t), \dots, X^{(d)}(t))$  solves the following SDE<sup>3</sup>

$$(2.4) \quad dX_t^{(i)} = a_i(\mathbf{X}_t)dt + \sum_{j=1}^d b_{ij}(\mathbf{X}_t)dW_t^{(j)}.$$

The use of the Brownian bridge construction for path simulation implies that  $\mathbf{W} := (W^{(1)}, \dots, W^{(d)})$  can be represented hierarchically as

$$W^{(j)}(t) = \frac{t}{T}W^{(j)}(T) + B^{(j)}(t) = \frac{t}{\sqrt{T}}Z_1^{(j)} + B^{(j)}(t), \quad 1 \leq j \leq d,$$

where  $\{Z_1^{(j)}\}_{j=1}^d$  are independent and identically distributed (i.i.d.) standard Gaussian random variables (rdvs), and  $\{B^{(j)}\}_{j=1}^d$  are independent Brownian bridges.

We denote by  $(Z_1^{(j)}, \dots, Z_N^{(j)})$  the  $N$  standard Gaussian independent rdvs used to construct the approximate path of the  $j$ -th asset  $\bar{X}^{(j)}$ , where  $N$  represents the number of time steps used in the discretization ( $\Delta t = \frac{T}{N}$ ).  $\psi^{(j)} : (Z_1^{(j)}, \dots, Z_N^{(j)}) \rightarrow (B_1^{(j)}, \dots, B_N^{(j)})$  denotes the mapping of the Brownian bridge construction, and  $\Phi : (\Delta t, \mathbf{B}) \rightarrow \bar{\mathbf{X}}^{\Delta t}(T)$  denotes the mapping of the time-stepping scheme, where  $\mathbf{B} := (B_1^{(1)}, \dots, B_N^{(1)}, \dots, B_1^{(d)}, \dots, B_N^{(d)})$  is the noncorrelated Brownian

<sup>2</sup>We present the monotonicity condition for an increasing function without any loss of generality.

<sup>3</sup>We assume that the  $\{W^{(j)}\}_{j=1}^d$  are uncorrelated and the correlation terms are included in the diffusion terms  $b_{ij}$ . Moreover, without restriction, the diffusion coefficients  $b_{ij}$  can be stochastic as well.

bridge<sup>4</sup> and  $\overline{\mathbf{X}}^{\Delta t}(T) := (\overline{X}_T^{(1)}, \dots, \overline{X}_T^{(d)})$ . Then, our quantity of interest can be expressed as

$$\begin{aligned}
\mathbb{E}[g(\mathbf{X}(T))] &\approx \mathbb{E}\left[g\left(\overline{X}_T^{(1)}, \dots, \overline{X}_T^{(d)}\right)\right] = \mathbb{E}\left[g(\overline{\mathbf{X}}^{\Delta t}(T))\right] \\
&= \mathbb{E}\left[g \circ \Phi\left(B_1^{(1)}, \dots, B_N^{(1)}, \dots, B_1^{(d)}, \dots, B_N^{(d)}\right)\right] \\
&= \mathbb{E}\left[g \circ \Phi\left(\psi^{(1)}(Z_1^{(1)}, \dots, Z_N^{(1)}), \dots, \psi^{(d)}(Z_1^{(d)}, \dots, Z_N^{(d)})\right)\right] \\
(2.5) \quad &= \int_{\mathbb{R}^{d \times N}} G(z_1^{(1)}, \dots, z_N^{(1)}, \dots, z_1^{(d)}, \dots, z_N^{(d)}) \rho_{d \times N}(\mathbf{z}) dz_1^{(1)} \dots dz_N^{(1)} \dots dz_1^{(d)} \dots dz_N^{(d)},
\end{aligned}$$

where  $G := g \circ \Phi \circ (\psi^{(1)}, \dots, \psi^{(d)})$  and  $\rho_{d \times N}$  represents the  $d \times N$  multivariate Gaussian density.

The discontinuity location is determined by solving the corresponding root-finding problem in one dimension after adopting suboptimal linear mapping for the coarsest factors of the Brownian increments  $\mathbf{Z}_1 := (Z_1^{(1)}, \dots, Z_1^{(d)})$

$$(2.6) \quad \mathbf{Y} = \mathcal{A}\mathbf{Z}_1,$$

where  $\mathcal{A}$  is a  $d \times d$  matrix representing the linear mapping.  $\mathcal{A}$  is generally selected from a family of rotations.

Considering that the irregularity is located at  $\phi(\overline{\mathbf{X}}^{\Delta t}(T)) = 0$  (see (2.1))<sup>5</sup>, for fixed  $\mathbf{y}_{-1}, \mathbf{z}_{-1}^{(1)}, \dots, \mathbf{z}_{-1}^{(d)}$ , we must find the roots of  $P(y_1^*)$  to determine the discontinuity location  $y_1^*$  (first component of  $\mathbf{y}$  in (2.6)):

$$\phi(\overline{\mathbf{X}}^{\Delta t}(T)) := P(y_1^*) = 0.$$

We used the Newton iteration method to determine the approximated discontinuity location  $\overline{y}_1^*$ .

Using (2.5), the second step of our numerical smoothing idea presented in [4] involves performing the numerical preintegration as follows:

$$\begin{aligned}
(2.7) \quad \mathbb{E}[g(\mathbf{X}(T))] &\approx \mathbb{E}\left[g\left(\overline{X}_T^{(1)}, \dots, \overline{X}_T^{(d)}\right)\right] := \mathbb{E}\left[I\left(\mathbf{Y}_{-1}, \mathbf{Z}_{-1}^{(1)}, \dots, \mathbf{Z}_{-1}^{(d)}\right)\right] \\
&\approx \mathbb{E}\left[\overline{I}\left(\mathbf{Y}_{-1}, \mathbf{Z}_{-1}^{(1)}, \dots, \mathbf{Z}_{-1}^{(d)}\right)\right],
\end{aligned}$$

where

$$\begin{aligned}
(2.8) \quad I\left(\mathbf{y}_{-1}, \mathbf{z}_{-1}^{(1)}, \dots, \mathbf{z}_{-1}^{(d)}\right) &= \int_{\mathbb{R}} G\left(y_1, \mathbf{y}_{-1}, \mathbf{z}_{-1}^{(1)}, \dots, \mathbf{z}_{-1}^{(d)}\right) \rho_1(y_1) dy_1 \\
&= \int_{-\infty}^{y_1^*} G\left(y_1, \mathbf{y}_{-1}, \mathbf{z}_{-1}^{(1)}, \dots, \mathbf{z}_{-1}^{(d)}\right) \rho_1(y_1) dy_1 + \int_{y_1^*}^{+\infty} G\left(y_1, \mathbf{y}_{-1}, \mathbf{z}_{-1}^{(1)}, \dots, \mathbf{z}_{-1}^{(d)}\right) \rho_1(y_1) dy_1,
\end{aligned}$$

and  $\overline{I}$  is the approximation of  $I$  obtained using the Newton iteration and a two-sided Laguerre quadrature rule. It is expressed as follows:

$$(2.9) \quad \overline{I}\left(\mathbf{y}_{-1}, \mathbf{z}_{-1}^{(1)}, \dots, \mathbf{z}_{-1}^{(d)}\right) := \sum_{k=0}^{M_{\text{Lag}}} \eta_k G\left(\zeta_k(\overline{y}_1^*), \mathbf{y}_{-1}, \mathbf{z}_{-1}^{(1)}, \dots, \mathbf{z}_{-1}^{(d)}\right),$$

<sup>4</sup>Without loss of generality, the correlated Brownian bridge can be obtained via simple matrix multiplication.

<sup>5</sup>The locations may differ depending on the considered observable.

where  $M_{\text{Lag}}$  represents the number of Laguerre quadrature points  $\zeta_k \in \mathbb{R}$  with  $\zeta_0 = \bar{y}_1^*$  and corresponding weights  $\eta_k$ <sup>6</sup>.

Formulas (2.8) and (2.9) can be easily extended to the case in which there are finite numerous discontinuities. We refer to Remark 2.4 presented in [4] for this extension.

### 2.3 Extending the numerical smoothing idea toward density estimation

In this subsection, we extend the numerical smoothing idea to approximate the density at point  $u$ ,  $\rho_{X_T}(u)$ , for the stochastic process  $X$ , at time  $T$ , whose dynamics is given by (2.4):

$$(2.10) \quad \rho_{X_T}(u) = \mathbb{E} [\delta(X(T) - u)].$$

For the one-dimensional case, by conditioning w.r.t. the Brownian bridge,  $B$ , we obtain

$$(2.11) \quad \begin{aligned} \rho_{X_T}(u) &= \mathbb{E} [\delta(X(T) - u)] \approx \mathbb{E} [\delta(\bar{X}^{\Delta t}(T) - u)] = \mathbb{E} \left[ \mathbb{E} [\delta(\bar{X}^{\Delta t}(T) - u) \mid B] \right] \\ &= \frac{1}{\sqrt{2\pi}} \mathbb{E} \left[ \exp \left( - (Y^*(u))^2 / 2 \right) \frac{dY^*}{dx}(u) \right] \\ &\approx \frac{1}{\sqrt{2\pi}} \mathbb{E} \left[ \exp \left( - (\bar{Y}^*(u))^2 / 2 \right) \frac{d\bar{Y}^*}{dx}(u) \right] \end{aligned}$$

where  $Y^*(u)$  and  $\bar{Y}^*(u)$  are the exact and approximate discontinuity locations, respectively, and obtained numerically by solving:  $\bar{X}^{\Delta t}(T; \bar{Y}^*(x), \mathbf{Z}_{-1}) = x$ , where  $\mathbf{Z}$  is the Gaussian random vector used for Brownian bridge construction.

Formula (2.11) can be generalized to the multidimensional case, with the difference that one needs to perform a root finding procedure in the  $d$ -dimensional space characterized by the coarsest factor in each dimension. Explicitly, for  $\mathbf{u} \in \mathbb{R}^d$

$$(2.12) \quad \begin{aligned} \rho_{\mathbf{X}_T}(\mathbf{u}) &= \mathbb{E} [\delta(\mathbf{X}(T) - \mathbf{u})] \approx \mathbb{E} [\delta(\bar{\mathbf{X}}^{\Delta t}(T) - \mathbf{u})] = \mathbb{E} [\rho_d(\mathbf{Y}^*(\mathbf{u})) \det(\mathbf{J}(\mathbf{u}))] := \mathbb{E} \left[ F \left( \mathbf{Y}_{-1}, \mathbf{Z}_{-1}^{(1)}, \dots, \mathbf{Z}_{-1}^{(d)}; \mathbf{u} \right) \right] \\ &\approx \mathbb{E} \left[ \rho_d(\bar{\mathbf{Y}}^*(\mathbf{u})) \det(\bar{\mathbf{J}}(\mathbf{u})) \right] \\ &:= \mathbb{E} \left[ \bar{F} \left( \mathbf{Y}_{-1}, \mathbf{Z}_{-1}^{(1)}, \dots, \mathbf{Z}_{-1}^{(d)}; \mathbf{u} \right) \right], \end{aligned}$$

where  $\mathbf{Y}^*(\mathbf{u})$  and  $\bar{\mathbf{Y}}^*(\mathbf{u})$  are the exact and approximate discontinuity locations, respectively, and obtained numerically by solving:  $\bar{\mathbf{X}}^{\Delta t}(T; \bar{\mathbf{Y}}^*(\mathbf{x}), \mathbf{Y}_{-1}, \mathbf{Z}_{-1}^{(1)}, \dots, \mathbf{Z}_{-1}^{(d)}) = \mathbf{x}$ .  $\mathbf{J}$  and  $\bar{\mathbf{J}}$  are the Jacobian matrices with  $\mathbf{J}_{ij} = \frac{\partial y_i^*}{\partial x_j}$  and  $\bar{\mathbf{J}} = \frac{\partial \bar{y}_i^*}{\partial x_j}$ .  $\det(\cdot)$  denotes the determinant of a matrix.

The numerical smoothing procedure presented in (2.11) and (2.12) enables the MLMC estimator (see Section 3) to compute density functions. We recall that MLMC without any smoothing will fail due to the infinite variance caused by the singularity of the delta function. Moreover, we emphasize that, owing to the exact conditional expectation w.r.t. the Brownian bridge, the only error present in our smoothing approach corresponds to the root-finding procedure for finding the discontinuity location, which does not depend exponentially on the dimension of the problem. As an alternative to our approach, one may use kernel density estimation techniques or a parametric

---

<sup>6</sup>Of course, the points  $\zeta_k$  must be selected in a systematic manner depending on  $\bar{y}_1^*$ .

smoothing approach as the one reported in [15]. However, this class of approaches has a pointwise error that increases exponentially w.r.t. the dimension of the state vector  $\mathbf{X}$  (or a vector-valued function that depends on the density of  $\mathbf{X}$ ). For instance, for a  $d$ -dimensional problem, the kernel density estimator with a bandwidth matrix,  $\mathcal{H} = \text{diag}(h, \dots, h)$ , has an MSE of the order of  $c_1 M^{-1} h^{-d} + c_2 h^4$ , where  $M$  is the number of samples and  $c_1$  and  $c_2$  are constants.

**Remark 2.1** (Extending numerical smoothing for density estimation to the case of multiple roots). For the case in which there are finite numerous discontinuities, (2.11) can be extended to (2.13)

$$(2.13) \quad \begin{aligned} \rho_{X_T}(u) = \mathbb{E}[\delta(X(T) - u)] &\approx \mathbb{E}\left[\delta(\bar{X}^{\Delta t}(T) - u)\right] = \frac{1}{\sqrt{2\pi}} \mathbb{E}\left[\sum_{i=1}^R \exp\left(-\frac{(Y_i^*(u))^2}{2}\right) \frac{dY_i^*(u)}{dx}\right] \\ &\approx \frac{1}{\sqrt{2\pi}} \sum_{i=1}^R \mathbb{E}\left[\exp\left(-\frac{(\bar{Y}_i^*(u))^2}{2}\right) \frac{d\bar{Y}_i^*(u)}{dx}\right], \end{aligned}$$

where  $\{Y_i^*(u)\}_{i=1}^R$  and  $\{\bar{Y}_i^*(u)\}_{i=1}^R$  are the exact and approximated discontinuity locations, respectively.

### 3 MLMC Combined with Numerical Smoothing

Using the MLMC method, as described in [12, 13], our approach aims to efficiently approximate the resulting expectation obtained after the numerical smoothing step, defined in (2.7) and (2.9), when  $g(\mathbf{x}) = \mathbf{1}_{(\phi(\mathbf{x}) \geq 0)}$ , or (2.11) and (2.12), when  $g(\mathbf{x}) = \delta(\phi(\mathbf{x}) = 0)$ .

We construct our MLMC estimator as follows: First, we consider a hierarchy of nested meshes of the time interval  $[0, T]$ , indexed by  $\ell = 0, 1, \dots, L$ .  $\Delta t_0$  denotes the step size used at level  $\ell = L_0$ . The size of the subsequent time steps for levels  $\ell \geq L_0 + 1$  is given by  $\Delta t_\ell = K^{-\ell} \Delta t_0$ , where  $K > 1$  is a given constant integer. In this work, we take  $K = 2$ . Moreover,  $M_{\text{Lag}, \ell}$  and  $\text{TOL}_{\text{Newton}, \ell}$  denote the number of Laguerre quadrature points and the tolerance of the Newton method at the level  $\ell$ , respectively. Hereafter, to simplify notation,  $\bar{I}_\ell$  corresponds to  $\bar{I}$  expressed in (2.9) (or  $\bar{F}$  expressed in (2.12), when estimating densities) computed using  $\Delta t_\ell$ ,  $\text{TOL}_{\text{Newton}, \ell}$  and  $M_{\text{Lag}, \ell}$ . Finally, we denote by  $M_\ell$  the number of samples at level  $\ell$ .

Consider now the following telescoping decomposition of  $\mathbb{E}[\bar{I}_L]$

$$\mathbb{E}[\bar{I}_L] = \mathbb{E}[\bar{I}_{L_0}] + \sum_{\ell=L_0+1}^L \mathbb{E}[\bar{I}_\ell - \bar{I}_{\ell-1}]$$

Then, by defining

$$(3.1) \quad \hat{Q}_0 := \frac{1}{M_0} \sum_{m_0=1}^{M_0} \bar{I}_{0, [m_0]}; \quad \hat{Q}_\ell := \frac{1}{M_\ell} \sum_{m_\ell=1}^{M_\ell} (\bar{I}_{\ell, [m_\ell]} - \bar{I}_{\ell-1, [m_\ell]}), \quad 1 \leq \ell \leq L,$$

we arrive at the unbiased MLMC estimator,  $\hat{Q}$ , of  $\mathbb{E}[\bar{I}_L]$

$$\hat{Q} := \sum_{\ell=L_0}^L \hat{Q}_\ell.$$

Notably, the key point in constructing (3.1) is that both  $\bar{I}_{\ell, [m_\ell]}$  and  $\bar{I}_{\ell-1, [m_\ell]}$  are sampled using different time discretizations but with the same generated randomness.

### 3.1 Error analysis

In this subsection, we analyze the different errors contributions in our approach that combines the MLMC estimator with the numerical smoothing to approximate  $\mathbb{E}[g(X(T))]$  with  $g$  given by (2.1). First, we discuss the case  $g(\mathbf{x}) = \mathbf{1}_{(\phi(\mathbf{x}) \geq 0)}$ . Then, we make particular observations in Remark 3.2 for the density estimation case. Following the notation of Sections 2 and 3, we obtain the following error decomposition

$$\begin{aligned}
\mathbb{E}[g(X(T))] - \widehat{Q} &= \underbrace{\mathbb{E}[g(X(T))] - \mathbb{E}\left[g(\bar{\mathbf{X}}^{\Delta t_L}(T))\right]}_{\text{Error I: bias or weak error}} \\
&\quad + \underbrace{\mathbb{E}\left[I_L\left(\mathbf{Y}_{-1}, \mathbf{Z}_{-1}^{(1)}, \dots, \mathbf{Z}_{-1}^{(d)}\right)\right] - \mathbb{E}\left[\bar{I}_L\left(\mathbf{Y}_{-1}, \mathbf{Z}_{-1}^{(1)}, \dots, \mathbf{Z}_{-1}^{(d)}\right)\right]}_{\text{Error II: numerical smoothing error}} \\
(3.2) \quad &\quad + \underbrace{\mathbb{E}\left[\bar{I}_L\left(\mathbf{Y}_{-1}, \mathbf{Z}_{-1}^{(1)}, \dots, \mathbf{Z}_{-1}^{(d)}\right)\right] - \widehat{Q}}_{\text{Error III: MLMC statistical error}},
\end{aligned}$$

where  $I_L$  corresponds to  $I$  expressed in (2.8) computed using  $\Delta t_\ell$ .

Because we use schemes based on forward Euler to simulate the dynamics of  $X$ , we obtain<sup>7</sup>

$$(3.3) \quad \text{Error I} = \mathcal{O}(\Delta t_L).$$

Error II in (3.2) was analyzed in [4], and is expressed as

$$\begin{aligned}
(3.4) \quad \text{Error II} &:= \mathbb{E}\left[I_L\left(\mathbf{Y}_{-1}, \mathbf{Z}_{-1}^{(1)}, \dots, \mathbf{Z}_{-1}^{(d)}\right)\right] - \mathbb{E}\left[\bar{I}_L\left(\mathbf{Y}_{-1}, \mathbf{Z}_{-1}^{(1)}, \dots, \mathbf{Z}_{-1}^{(d)}\right)\right] \\
&= \mathcal{O}\left(M_{\text{Lag}, L}^{-s}\right) + \mathcal{O}\left(\text{TOL}_{\text{Newton}, L}^{\eta+1}\right),
\end{aligned}$$

where  $\eta \geq 0^8$  and  $s > 0$  is related to the degree of regularity of the integrand,  $G$ , w.r.t.  $y_1$ .<sup>9</sup>

Because  $\widehat{Q}$  is an unbiased MLMC estimator of  $\mathbb{E}\left[\bar{I}_L\left(\mathbf{Y}_{-1}, \mathbf{Z}_{-1}^{(1)}, \dots, \mathbf{Z}_{-1}^{(d)}\right)\right]$ , then Error III presents the corresponding statistical error. From the standard multilevel analysis (see [12, 13]), we obtain

$$(3.5) \quad \text{Error III} \propto \sqrt{\sum_{\ell=L_0}^L (M_\ell^*)^{-1} V_\ell} = \sqrt{\sum_{\ell=L_0}^L \sqrt{C_\ell V_\ell}},$$

where  $M_\ell^*$  is the optimal number of samples per level,

$$V_{L_0} := \text{Var}\left[\bar{I}_0\right], \quad V_\ell := \text{Var}\left[\bar{I}_\ell - \bar{I}_{\ell-1}\right], \quad L_0 + 1 \leq \ell \leq L,$$

<sup>7</sup>In general, Error I =  $\mathcal{O}(\Delta t_L^\alpha)$ , with  $\alpha \geq 0$ . In particular,  $\alpha > 1$  for higher order schemes.

<sup>8</sup>The value of  $\eta$  depends on the structure of  $g$ : for instance,  $\eta = 0$  for  $g(\mathbf{x}) = \mathbf{1}_{(\phi(\mathbf{x}) \geq 0)}$ .

<sup>9</sup>In this case, the derivatives of  $G$  w.r.t.  $y_1$  are bounded up to order  $s$ .

and  $C_\ell$  is the cost per sample per level. In our context, it is given by

$$(3.6) \quad C_\ell \propto (\Delta t_\ell)^{-1} (M_{\text{Lag},\ell} + N_{\text{iter},\ell}) \propto (\Delta t_\ell)^{-1} \left( M_{\text{Lag},\ell} + \log \left( \text{TOL}_{\text{Newton},\ell}^{-1} \right) \right),$$

where  $N_{\text{iter},\ell}$  is the number of the Newton iterations at level  $\ell$ .<sup>10</sup>

Moreover, estimates of the variances  $\{V_\ell\}_{\ell=L_0+1}^L$  are given by Corollary 3.1 (please refer to Section 4 for more numerical illustrations).

**Corollary 3.1.** *Under the assumptions of Theorem 3.1 in [4], the integrand  $\bar{I}$  in (2.7) is Lipschitz, and*

$$(3.7) \quad V_\ell = \mathcal{O}(\Delta t_\ell).$$

*Proof.* Using Theorem 3.1 presented in [4], we obtain that  $\bar{I}$  in (2.7) is  $C^\infty$ . Therefore, it is Lipschitz with constant  $L_{\bar{I}}$ . Since we use Euler schemes, we obtain

$$V_\ell := \text{Var} [\bar{I}_\ell - \bar{I}_{\ell-1}] \leq \text{E} \left[ (\bar{I}_\ell - \bar{I}_{\ell-1})^2 \right] \leq L_{\bar{I}}^2 \text{E} \left[ (\bar{X}_\ell(T) - \bar{X}_{\ell-1}(T))^2 \right] = \mathcal{O}(\Delta t_\ell).^{11} \quad \square$$

Therefore, using (3.5), (3.6) and (3.7), we obtain

$$(3.8) \quad \text{Error III} = \mathcal{O} \left( \sqrt{\sum_{\ell=L_0}^L \sqrt{M_{\text{Lag},\ell} + \log \left( \text{TOL}_{\text{Newton},\ell}^{-1} \right)}} \right).$$

Given (3.2), (3.3), (3.4) and (3.8), the total error estimate of our approach is

$$(3.9) \quad \begin{aligned} \mathcal{E}_{\text{total}} &:= \text{E} [g(X(T))] - \hat{Q} \\ &= \mathcal{O}(\Delta t_L) + \mathcal{O} \left( \sqrt{\sum_{\ell=L_0}^L \sqrt{M_{\text{Lag},\ell} + \log \left( \text{TOL}_{\text{Newton},\ell}^{-1} \right)}} \right) + \mathcal{O} \left( M_{\text{Lag},L}^{-s} \right) + \mathcal{O} \left( \text{TOL}_{\text{Newton},L}^{\eta+1} \right). \end{aligned}$$

**Remark 3.2** (Error discussion when estimating densities). For the density estimation case, we have the same error structure as given in (3.9) with the only difference that we do not have the term  $\mathcal{O} \left( M_{\text{Lag},L}^{-s} \right)$  because we do not perform any numerical pre-integration.

### 3.2 Work and complexity analysis

From the MLMC analysis presented in [13] and from (3.6) and (3.7), we obtain an estimate of the work of our approach as follows:

$$(3.10) \quad \begin{aligned} \text{Work} (L, L_0, \{M_{\text{Lag},\ell}\}_{\ell=L_0}^L, \{\text{TOL}_{\text{Newton},\ell}\}_{\ell=L_0}^L) &\propto \sum_{\ell=L_0}^L M_\ell^* C_\ell \propto \sum_{\ell=L_0}^L \sqrt{C_\ell V_\ell} \\ &\propto \sum_{\ell=L_0}^L \sqrt{M_{\text{Lag},\ell} + \log \left( \text{TOL}_{\text{Newton},\ell}^{-1} \right)}. \end{aligned}$$

---

<sup>10</sup>Under some mild conditions and using Taylor expansion, we can show that Newton iteration has a second order convergence and conclude that  $N_{\text{iter},\ell} \propto \log \left( \text{TOL}_{\text{Newton},\ell}^{-1} \right)$ .

<sup>11</sup>The constant in  $\mathcal{O}(\Delta t_\ell)$  depends on  $M_{\text{Lag},\ell}$  and  $\text{TOL}_{\text{Newton},\ell}$ . Investigating this dependence is out of the scope of this work.

To achieve a certain error tolerance, TOL, with an optimal performance of our approach, one needs to solve (3.11) using (3.9) and (3.10)

$$(3.11) \quad \begin{cases} \min & \text{Work}(L, L_0, \{M_{\text{Lag}, \ell}\}_{\ell=L_0}^L, \{\text{TOL}_{\text{Newton}, \ell}\}_{\ell=L_0}^L) \\ \text{s.t. } & \mathcal{E}_{\text{total}} = \text{TOL} \end{cases}$$

In this work, we do not solve (3.11); however, we select the different parameters heuristically<sup>12</sup>. A further investigation of optimizing (3.11) is left for a future study.

In Corollary 3.3, we state the complexity of our approach, MLMC combined with numerical smoothing, compared with MLMC without smoothing.

**Corollary 3.3.** *Under the assumptions of Theorem 3.1 in [4], the complexity of MLMC combined with numerical smoothing using Euler discretization is  $\mathcal{O}\left(\text{TOL}^{-2}(\log(\text{TOL}))^2\right)$  compared with  $\mathcal{O}\left(\text{TOL}^{-2.5}\right)$  for MLMC without smoothing.*

*Proof.* Theorem 1 presented in [13] (see also Theorem 1 given in [10]) derives the computational complexity of the MLMC estimator under different scenarios, depending on the values of  $\alpha$  (weak convergence rate),  $\beta$  (variance decay rate), and  $\gamma$  (work rate). For the Euler scheme, and for scenarios with or without numerical smoothing, we have  $\gamma = 1$ . For non-Lipschitz payoffs and without smoothing, e.g., for digital and barrier options,  $V_\ell = \mathcal{O}\left(\Delta t_\ell^{1/2}\right)$  (see [14, 3, 13]), i.e.,  $\beta = 1/2$ . Thus, we obtain the worst-case complexity of the MLMC estimator, i.e.,  $\mathcal{O}\left(\text{TOL}^{-2.5}\right)$ . For our approach based on the numerical smoothing idea, and by Corollary 3.1, we recover  $\beta = 1$ , implying an MLMC complexity of  $\mathcal{O}\left(\text{TOL}^{-2}(\log(\text{TOL}))^2\right)$ .  $\square$

**Remark 3.4** (About high-order schemes). For non-Lipschitz observables, high-order schemes, such as the Milstein scheme, can improve the variance decay rate [22, 13] as compared with the Euler scheme, thus improving the MLMC estimator's complexity without the need for a smoothing procedure. However, this possibility comes with some disadvantages compared to our approach: (i) for high-dimensional dynamics, coupling issues may arise and the scheme becomes computationally expensive and (ii) the deterioration of the robustness of the MLMC estimator because the kurtosis explodes as  $\Delta t$  decreases (deep levels of MLMC), of order  $\mathcal{O}\left(\Delta t_\ell^{-1}\right)$  compared with  $\mathcal{O}\left(\Delta t_\ell^{-1/2}\right)$  for Euler without smoothing [15] and  $\mathcal{O}(1)$  for our approach (see Subsection 3.3 and Section 4).

### 3.3 Robustness analysis

When approximating the expectation of nonsmooth (non-Lipschitz) observables, e.g., for options pricing or density estimation of asset price dynamics, the standard MLMC estimator (without smoothing) suffers from poor robustness and performance owing to high kurtosis at deep levels (small  $\Delta t_\ell$ ). To explain this undesirable feature, let  $g$  denote an rdv and let  $g_\ell$  denote the corresponding level  $\ell$  numerical approximation. Further, we define  $Y_\ell := g_\ell - g_{\ell-1}$ . The standard deviation of the sample variance for the rdv  $Y_\ell$  is given by

$$(3.12) \quad \sigma_{S^2(Y_\ell)} = \frac{\text{Var}[Y_\ell]}{\sqrt{M_\ell}} \sqrt{(\bar{\kappa}_\ell - 1) + \frac{2}{M_\ell - 1}}, \quad L_0 + 1 \leq \ell \leq L,$$

<sup>12</sup>In our numerical experiments, we select  $L_0$  such that  $\text{Var}[\bar{I}_{L_0+1} - \bar{I}_{L_0}] \ll \text{Var}[\bar{I}_{L_0}]$ , in order to ensure the stability of the variance of the coupled paths of our MLMC estimator.

where  $\bar{\kappa}_\ell$  is the kurtosis at level  $\ell$ , given by

$$(3.13) \quad \bar{\kappa}_\ell = \frac{\mathbb{E} \left[ (Y_\ell - \mathbb{E}[Y_\ell])^4 \right]}{(\text{Var}[Y_\ell])^2}, \quad L_0 + 1 \leq \ell \leq L.$$

We recall that in the MLMC setting, accurate estimates of  $\bar{V}_\ell = \text{Var}[Y_\ell]$  are required because the optimal number of samples per level,  $M_\ell^*$ , for the multilevel estimator is given by

$$M_\ell^* \propto \sqrt{\bar{V}_\ell \bar{C}_\ell^{-1}} \sum_{\ell=L_0}^L \sqrt{\bar{V}_\ell \bar{C}_\ell}, \quad L_0 + 1 \leq \ell \leq L,$$

where  $\bar{C}_\ell$  is the cost per sample path per level.

From (3.12),  $\mathcal{O}(\bar{\kappa}_\ell)$  samples are required to obtain a reasonable estimate of the variance  $\bar{V}_\ell$ . Two possible consequences of the high kurtosis may occur, thus deteriorating the robustness and performance of the MLMC estimator

- The sample variance,  $\bar{V}_\ell$ , is underestimated (not reliable). Then, the required semilength of confidence interval is not faithfully attained owing to  $\sigma_{\mathcal{S}^2(Y_\ell)}$  given by (3.12).
- The sample variance,  $\bar{V}_\ell$ , is overestimated. In this case, too many sample paths are generated and the algorithm takes substantially more time to run.

In our context, when using the Euler scheme, the kurtosis at level  $\ell$  for the MLMC without numerical smoothing is of the order of  $\mathcal{O}(\Delta t_\ell^{-1/2})$  [15]. However, thanks to our numerical smoothing idea, the kurtosis at level  $\ell$  for our approach is of the order of  $\mathcal{O}(1)$ , as shown in Corollary 3.5 (please refer to Section 4 for more numerical illustrations of these behaviors).

**Corollary 3.5.** *Let  $\kappa_\ell$  be the kurtosis of the random variable  $Y_\ell := \bar{I}_\ell - \bar{I}_{\ell-1}$  ( $\bar{I}_\ell$  is defined in Section 3 using the Euler scheme), then, under the assumptions of Theorem 3.1 in [4], we obtain*

$$(3.14) \quad \kappa_\ell = \mathcal{O}(1).$$

*Proof.* Using Corollary 3.1, we obtain that  $\bar{I}$  is Lipschitz, and thus  $(\text{Var}[Y_\ell])^2 = \mathcal{O}(\Delta t_\ell^2)$ . Moreover, assuming some global Lipschitz conditions for the drift and diffusion of the SDE (2.4), then, using the  $L_p$  moment estimates result from [7], it is straightforward that  $\mathbb{E} \left[ (Y_\ell - \mathbb{E}[Y_\ell])^4 \right] = \mathcal{O}(\Delta t_\ell^2)$ . Therefore, using (3.13), we obtain the desired result presented in (3.14).  $\square$

## 4 Numerical Experiments

In this section, we numerically illustrate the advantages of combining the numerical smoothing idea with MLMC when (i) computing the price of a digital option (see Subsection 4.1) and (ii) approximating the density function of asset dynamics (see Subsection 4.2). We perform our tests for the discretized GBM (a didactic example) and the Heston model [18, 8, 19, 2], whose dynamics is given as follows

$$(4.1) \quad \begin{aligned} dX_t &= \mu X_t dt + \rho \sqrt{v_t} X_t dW_t^v + \sqrt{1 - \rho^2} \sqrt{v_t} X_t dW_t \\ dv_t &= \zeta(\theta - v_t) dt + \xi \sqrt{v_t} dW_t^v, \end{aligned}$$

where  $X_t$  denotes the asset price;  $v_t$  represents the instantaneous variance;  $(W_t^S, W_t^v)$  are the correlated Wiener processes with correlation  $\rho$ ;  $\mu$  represents the asset's rate of return;  $\theta$  is the mean variance;  $\zeta$  is the rate at which  $v_t$  reverts to  $\theta$ ; and  $\xi$  denotes the volatility of the volatility.

We use the Euler–Maruyama scheme to simulate the GBM dynamics. For simulating the Heston model, we use (i) the full truncation (FT) scheme [21] and (ii) the scheme based on simulating the volatility process as the sum of Ornstein–Uhlenbeck processes (OU scheme) (see Appendix C.3 presented in [4]). In our examples, we compare (i) the standard MLMC estimator (without smoothing) and (ii) our MLMC estimator combined with numerical smoothing (as explained in Sections 2 and 3). We note that in Figures 4.1, 4.2, 4.4, 4.5, 4.6, 4.8, and 4.10,  $P_\ell$  denotes the numerical approximation of our quantity of interest at level  $\ell$  of the MLMC estimator. In particular,  $P_\ell = \bar{I}_\ell$  when using numerical smoothing. Furthermore, our numerical experiments were produced using MATLAB (version R2021b) on a 3,2-GHz 8-Core Intel Xeon W architecture.

## 4.1 Pricing digital options

We aim to approximate the price of digital options, *i.e.*, we want to approximate

$$(4.2) \quad \mathbb{E}[g(X(T))] = \mathbb{E}[\mathbf{1}_{X(T) > K}],$$

where  $X(T)$  is the asset price at the maturity  $T$  and  $K$  is the strike price.

### 4.1.1 Pricing digital option under the GBM model

We price the digital option presented in (4.2) under the GBM model, with parameters:  $X_0 = K = 100$ ,  $T = 1$ , and  $\sigma = 0.2$ . Table 4.1 summarizes the obtained results for approximating the option price. More details are illustrated in Figures 4.1, 4.2, and 4.3. From these figures and Table 4.1, we obtain two main results:

1. A substantial reduction of the kurtosis at the finest level,  $\kappa_L$ , of the MLMC algorithm using the numerical smoothing. The kurtosis becomes bounded and is reduced by a factor of 236 (compare the bottom right plots presented in Figures 4.1 and 4.2). We emphasize that this is an important improvement regarding the robustness and performance of the MLMC estimator, as explained in Subsection 3.3.
2. Numerical smoothing considerably reduces the variance of the coupled levels in MLMC and improves the variance decay rate, from  $\beta = 1/2$  to  $\beta = 1$  (compare the top left plots in Figures 4.1 and 4.2), resulting in a reduction in the order of MLMC numerical complexity from  $\mathcal{O}(\text{TOL}^{-2.5})$  to  $\mathcal{O}(\text{TOL}^{-2}(\log(\text{TOL}))^2)$  (see Figure 4.3). Figure 4.3 shows that MLMC combined with numerical smoothing considerably outperforms standard MLMC in computational work, especially for small tolerances.

**Remark 4.1.** Notably, for the particular case of the GBM dynamics, a decaying variance of  $P_\ell$  in the top left plot presented in Figure 4.2 is expected to be observed because we use a Brownian bridge for path construction. Additionally, the integrand only depends on the terminal value of the Brownian bridge, which has a variance scale of the order  $\Delta t$ . Therefore, for this particular case, we expect the numerical complexity of the MC method with smoothing to be of the order of  $\mathcal{O}(\text{TOL}^{-2})$ . Note that this feature does not hold anymore for the Heston model as shown later.

Method	$\kappa_L$	$\alpha$	$\beta$	$\gamma$	Numerical complexity
MLMC without smoothing	709	1	1/2	1	$\mathcal{O}(\text{TOL}^{-2.5})$
MLMC with numerical smoothing	3	1	1	1	$\mathcal{O}(\text{TOL}^{-2}(\log(\text{TOL}))^2)$

Table 4.1: Digital option under the GBM model: summary of the MLMC results.  $\kappa_L$  is the kurtosis at the finest level, and  $(\alpha, \beta, \gamma)$  denote the weak, variance decay, and work rates, respectively. TOL is the user-selected tolerance. These results correspond to Figures 4.1, 4.2, and 4.3 respectively.

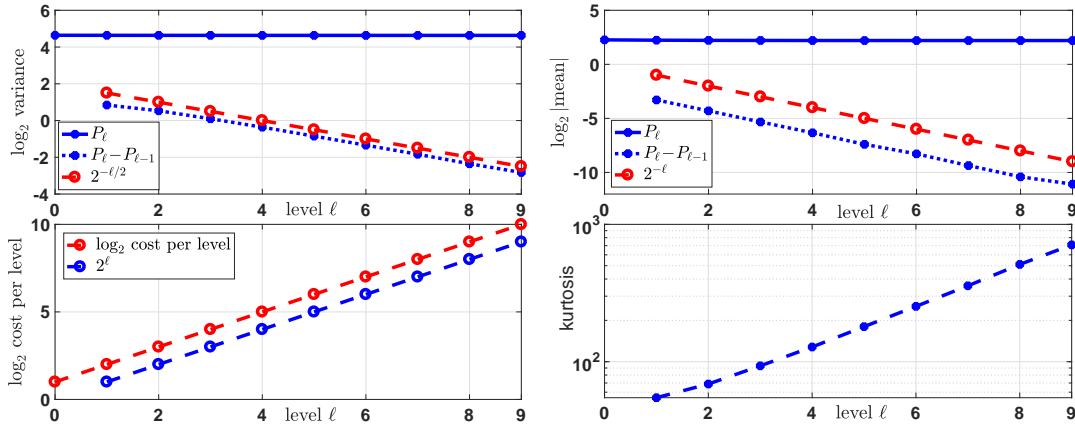


Figure 4.1: Digital option under the GBM model: convergence plots for MLMC without smoothing, combined with Euler–Maruyama discretization.

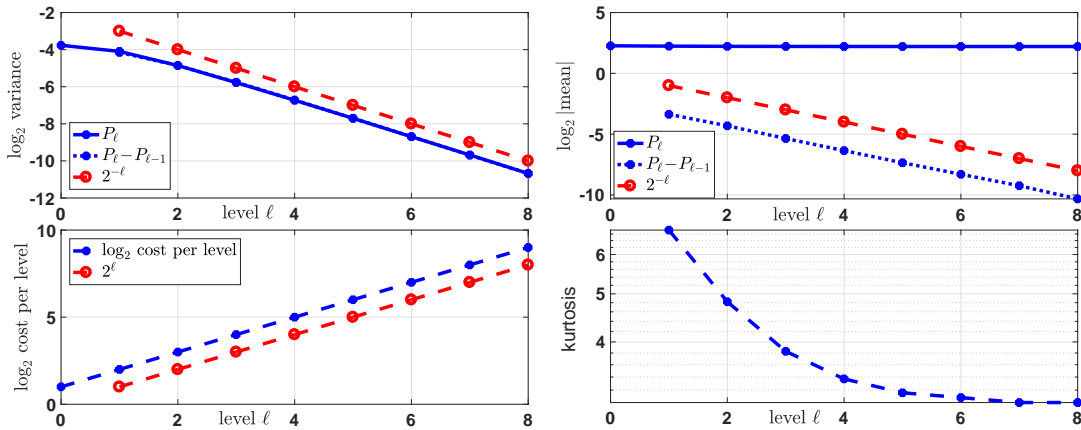


Figure 4.2: Digital option under the GBM model: convergence plots for MLMC with numerical smoothing ( $\text{TOL}_{\text{Newton},\ell} = 10^{-3}$ ,  $M_{\text{Lag},\ell} = 8$ ), combined with Euler–Maruyama discretization.

#### 4.1.2 Pricing digital option under the Heston model

We price the digital option presented in (4.2) under the Heston model (4.1), with parameters:  $T = 1$ ,  $X_0 = K = 100$ ,  $v_0 = 0.04$ ,  $\mu = 0$ ,  $\rho = -0.9$ ,  $\zeta = 1$ ,  $\xi = 0.1$ , and  $\theta = 0.0025$ . Table 4.2 summarizes

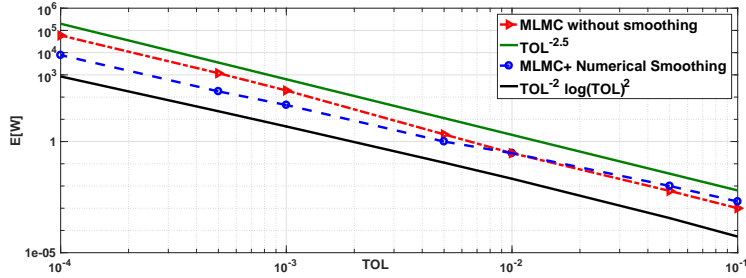


Figure 4.3: Digital option under the GBM model: comparison of the numerical complexity (expected work,  $E[W]$ , vs tolerance, TOL, in a log–log scale) of (i) standard MLMC, and (ii) MLMC with numerical smoothing. MLMC combined with numerical smoothing outperforms the MLMC without smoothing. Further, it achieves a better numerical complexity rate, *i.e.*,  $\mathcal{O}(\text{TOL}^{-2} \log(\text{TOL})^2)$ .

the obtained results for approximating the price in Table 4.2. More details are illustrated in Figures 4.4, 4.5, 4.6, and 4.7. From these figures and Table 4.2, we obtain the following results:

1. The substantial reduction of the kurtosis at the finest level,  $\kappa_L$ , of MLMC when using numerical smoothing (employing the OU-based or FT scheme). The kurtosis is bounded and reduced by a factor of  $> 27$  (compare the bottom right plots presented in Figures 4.4, 4.5, and 4.6). We emphasize that this is an important improvement regarding the robustness and performance of the MLMC estimator, as explained in Subsection 3.3.
2. Numerical smoothing (with OU-based or FT schemes) considerably reduces the variance of coupled levels in MLMC. Further, it improves the variance decay rate from  $\beta = 1/2$  to  $\beta = 1$  (compare the top left plots presented in Figures 4.4, 4.5, and 4.6), implying an improvement of the computational work and the order of MLMC numerical complexity from  $\mathcal{O}(\text{TOL}^{-2.5})$  to  $\mathcal{O}(\text{TOL}^{-2} (\log(\text{TOL}))^2)$  (see Figure 4.7).

Method	$\kappa_L$	$\alpha$	$\beta$	$\gamma$	Numerical complexity
MLMC without smoothing + FT scheme	245	1	1/2	1	$\mathcal{O}(\text{TOL}^{-2.5})$
MLMC with numerical smoothing + OU-based scheme	7	1	1	1	$\mathcal{O}(\text{TOL}^{-2} \log(\text{TOL})^2)$
MLMC with numerical smoothing+ FT scheme	9	1	1	1	$\mathcal{O}(\text{TOL}^{-2} \log(\text{TOL})^2)$

Table 4.2: Digital option under the Heston model: summary of the MLMC numerical results.  $\kappa_L$  is the kurtosis at the finest level of MLMC, and  $(\alpha, \beta, \gamma)$  present the weak, variance decay, and work rates, respectively. TOL is the user-selected tolerance. These results correspond to Figures 4.4, 4.5, 4.6, and 4.7.

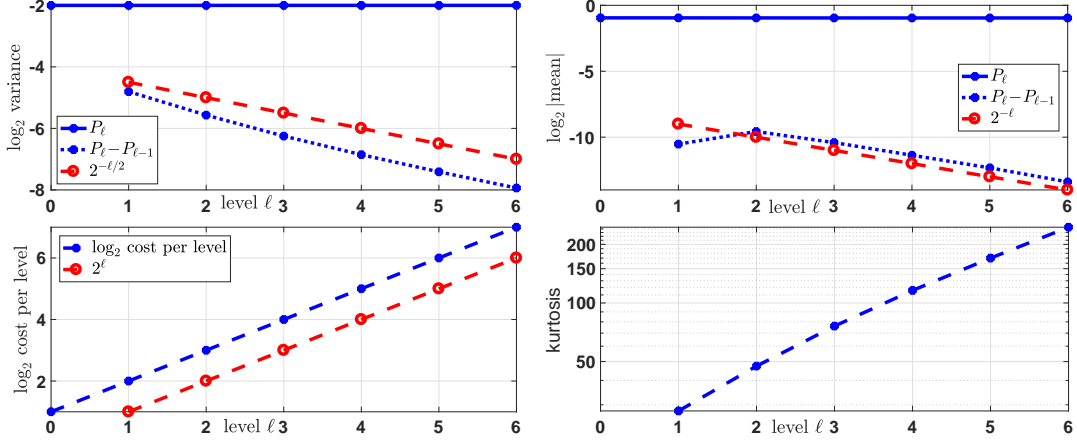


Figure 4.4: Digital option under Heston: Convergence plots for MLMC without smoothing, combined with the FT scheme.

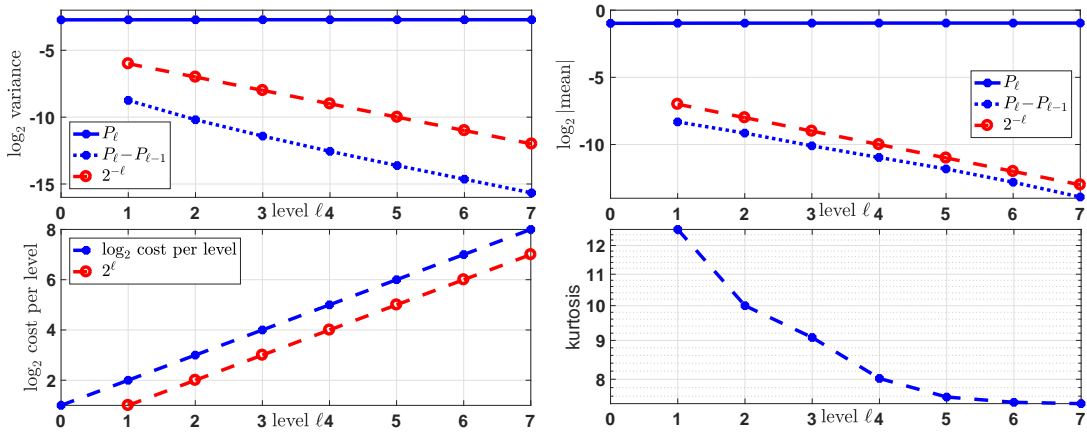


Figure 4.5: Digital option under the Heston model: convergence plots for MLMC with numerical smoothing ( $\text{TOL}_{\text{Newton}, \ell} = 10^{-3}$ ,  $M_{\text{lag}, \ell} = 32$ ), combined with the OU scheme.

## 4.2 Densities approximation

### 4.2.1 Density approximation under the GBM model

We compute the density  $\rho_{X(T)}$ , given by (2.10), at  $u = 1$  such that  $X$  is a GBM with parameters:  $X_0 = 1$ ,  $T = 1$ , and  $\sigma = 0.2$ . In this case, we know that  $X(T)$  is lognormally distributed with parameters  $-\sigma^2/2$  and  $\sigma$ .

Table 4.3 summarizes the results of MLMC combined with numerical smoothing. Figure 4.8 shows the detailed convergence, where we verify that the variance decay rate is of order one (see the top left plot presented in Figure 4.8), resulting in a numerical complexity of the MLMC estimator to be of the order of  $\mathcal{O}(\text{TOL}^{-2} (\log(\text{TOL}))^2)$ , as confirmed by Figure 4.9.

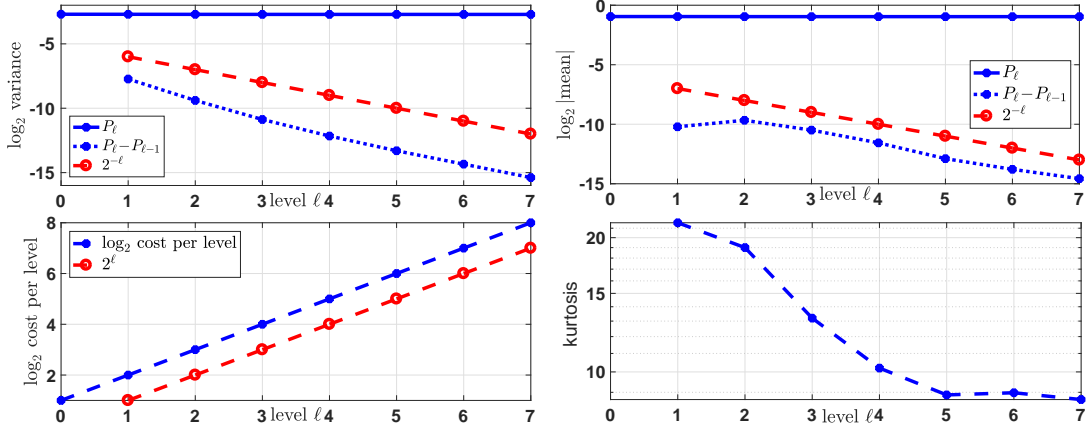


Figure 4.6: Digital option under the Heston model: convergence plots for MLMC with numerical smoothing ( $\text{TOL}_{\text{Newton},\ell} = 10^{-3}$ ,  $M_{\text{lag},\ell} = 32$ ), combined with the FT scheme.

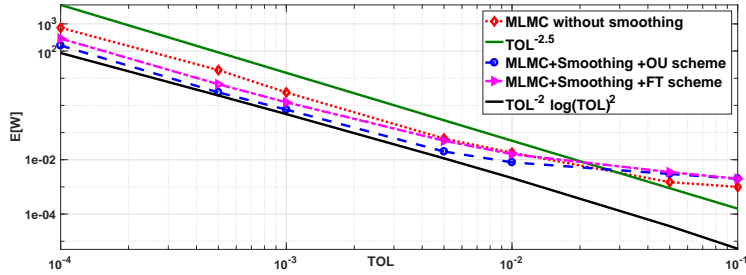


Figure 4.7: Digital option under the Heston model: comparison of the numerical complexity (expected work,  $E[W]$ , vs tolerance,  $\text{TOL}$ , in a log–log scale) of the (i) standard MLMC without smoothing (based on the FT scheme), (ii) MLMC with numerical smoothing (based on the OU scheme), and (iii) MLMC with numerical smoothing (based on the FT scheme). MLMC combined with numerical smoothing outperforms standard MLMC. Further, it achieves a better numerical complexity rate.

Method	$\kappa_L$	$\alpha$	$\beta$	$\gamma$	Numerical complexity
MLMC + numerical smoothing	5	1	1	1	$\mathcal{O}\left(\text{TOL}^{-2} (\log(\text{TOL}))^2\right)$

Table 4.3: Density of GBM: summary of the MLMC numerical results observed for computing the density  $\rho_{X(T)}$  at  $u = 1$ , where  $X$  follows the GBM dynamics.  $\kappa_L$  is the kurtosis at the finest level of MLMC, and  $(\alpha, \beta, \gamma)$  present the weak, variance decay, and work rates, respectively.  $\text{TOL}$  is the user-selected tolerance. These results correspond to Figures 4.8 and 4.9.

#### 4.2.2 Density Approximation under the Heston model

We compute the density  $\rho_{X(T)}$ , given by (2.10), at  $u = 1$  such that  $X$  is a Heston asset (4.1), with parameters:  $X_0 = 1$ ,  $v_0 = 0.04$ ,  $\mu = 0$ ,  $\rho = -0.9$ ,  $\zeta = 1$ ,  $\xi = 0.1$ , and  $\theta = 0.0025$ . In this case,

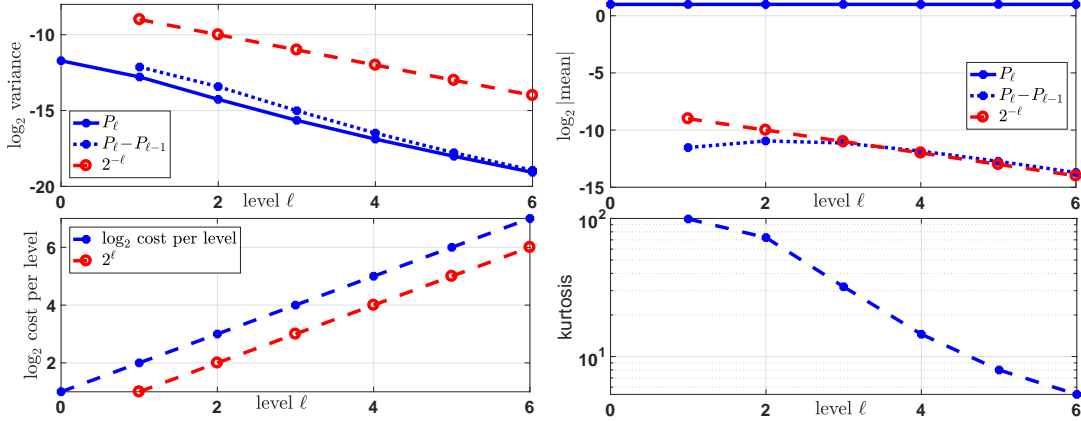


Figure 4.8: Density of GBM: convergence plots for MLMC with numerical smoothing ( $\text{TOL}_{\text{Newton},\ell} = 10^{-2}$ ) for computing the density  $\rho_{X(T)}$  at  $u = 1$ , where  $X$  follows the GBM dynamics. Remark 4.1 also holds in this example.

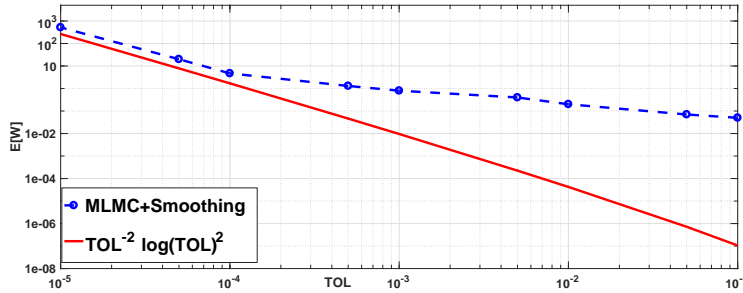


Figure 4.9: Density of GBM: numerical complexity of MLMC with numerical smoothing for computing the density  $\rho_{X(T)}$  at  $u = 1$ , where  $X$  follows the GBM dynamics.

as a reference solution, we obtain the density by applying the fractional Fourier transform to the characteristic function. Table 4.4 summarizes the obtained results. Figure 4.10 shows the detailed convergence results for the MLMC estimator combined with the numerical smoothing, using the OU scheme. This figure verifies that we obtain a variance decay rate of order one (see the top left plot presented in Figure 4.10), resulting in a numerical complexity of the MLMC estimator of the order of  $\mathcal{O}\left(\text{TOL}^{-2} (\log(\text{TOL}))^2\right)$ , as confirmed in Figure 4.11.

**Acknowledgments** C. Bayer gratefully acknowledges support from the German Research Foundation (DFG), via the Cluster of Excellence MATH+ (project AA4-2). This publication is based upon work supported by the King Abdullah University of Science and Technology (KAUST) Office of Sponsored Research (OSR) under Award No. OSR-2019-CRG8-4033, and the Alexander von Humboldt Foundation.

Method	$\kappa_L$	$\alpha$	$\beta$	$\gamma$	Numerical complexity
MLMC with numerical smoothing + OU-based scheme	8	1	1	1	$\mathcal{O}\left(\text{TOL}^{-2} (\log(\text{TOL}))^2\right)$

Table 4.4: Density of Heston: summary of the MLMC numerical results observed for computing the density  $\rho_{X(T)}$  at  $u = 1$ , where  $X$  follows the Heston dynamics.  $\kappa_L$  is the kurtosis at the finest level of MLMC,  $(\alpha, \beta, \gamma)$  present the weak, variance decay, and work rates, respectively. TOL is the user-selected tolerance. These results correspond to Figures 4.10 and 4.11.

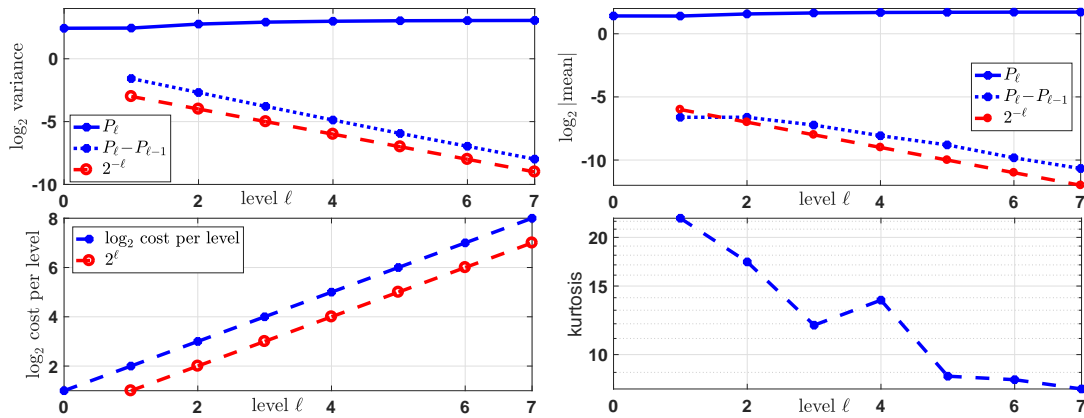


Figure 4.10: Density of Heston: Convergence plots for MLMC with numerical smoothing ( $\text{TOL}_{\text{Newton},\ell} = 10^{-2}$ ) combined with the OU scheme, for computing the density  $\rho_{X(T)}$  at  $u = 1$ , where  $X$  follows the Heston dynamics.

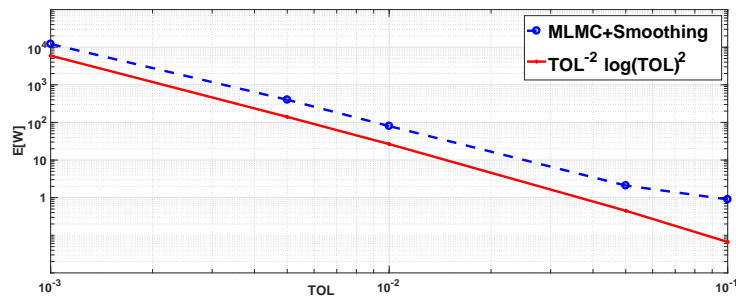


Figure 4.11: Density of Heston: Numerical complexity (expected work,  $E[W]$ , vs tolerance, TOL) of MLMC with numerical smoothing and combined with the OU scheme for computing for computing the density  $\rho_{X(T)}$  at  $u = 1$ , where  $X$  follows the Heston dynamics.

## References Cited

- [1] Martin Altmayer and Andreas Neuenkirch. Multilevel Monte Carlo quadrature of discontinuous payoffs in the generalized Heston model using Malliavin integration by parts. *SIAM Journal on Financial Mathematics : SIFIN*, 6(1):22–52, 2015. Online-Ressource.

- [2] Leif BG Andersen. Efficient simulation of the Heston stochastic volatility model. *Available at SSRN 946405*, 2007.
- [3] Rainer Avikainen. On irregular functionals of SDEs and the Euler scheme. *Finance and Stochastics*, 13(3):381–401, 2009.
- [4] Christian Bayer, Chiheb Ben Hammouda, and Raúl Tempone. Numerical smoothing with hierarchical adaptive sparse grids and quasi-Monte Carlo methods for efficient option pricing. *arXiv preprint arXiv:2111.01874*, 2021.
- [5] Chiheb Ben Hammouda, Nadhir Ben Rached, and Raúl Tempone. Importance sampling for a robust and efficient multilevel Monte Carlo estimator for stochastic reaction networks. *Statistics and Computing*, 30(6):1665–1689, 2020.
- [6] Chiheb Ben Hammouda, Alvaro Moraes, and Raúl Tempone. Multilevel hybrid split-step implicit tau-leap. *Numerical Algorithms*, 74(2):527–560, 2017.
- [7] Nicolas Bouleau and Dominique Lepingue. *Numerical methods for stochastic processes*, volume 273. John Wiley & Sons, 1994.
- [8] Mark Broadie and Özgür Kaya. Exact simulation of stochastic volatility and other affine jump diffusion processes. *Operations research*, 54(2):217–231, 2006.
- [9] Sylvestre Burgos and MB Giles. The computation of Greeks with multilevel Monte Carlo. *arXiv preprint arXiv:1102.1348*, 2011.
- [10] K Andrew Cliffe, Mike B Giles, Robert Scheichl, and Aretha L Teckentrup. Multilevel Monte Carlo methods and applications to elliptic PDEs with random coefficients. *Computing and Visualization in Science*, 14(1):3, 2011.
- [11] Michael B Giles. Improved multilevel Monte Carlo convergence using the Milstein scheme. In *Monte Carlo and Quasi-Monte Carlo Methods 2006*, pages 343–358. Springer, 2008.
- [12] Michael B Giles. Multilevel Monte Carlo path simulation. *Operations Research*, 56(3):607–617, 2008.
- [13] Michael B Giles. Multilevel Monte Carlo methods. *Acta Numerica*, 24:259–328, 2015.
- [14] Michael B Giles, Desmond J Higham, and Xuerong Mao. Analysing multi-level Monte Carlo for options with non-globally Lipschitz payoff. *Finance and Stochastics*, 13(3):403–413, 2009.
- [15] Michael B Giles, Tigran Nagapetyan, and Klaus Ritter. Multilevel Monte Carlo approximation of distribution functions and densities. *SIAM/ASA Journal on Uncertainty Quantification*, 3(1):267–295, 2015.
- [16] Wenhui Gou. Estimating value-at-risk using multilevel Monte Carlo maximum entropy method. Master’s thesis, University of Oxford, 2016.
- [17] Abdul-Lateef Haji-Ali, Jonathan Spence, and Aretha Teckentrup. Adaptive multilevel Monte Carlo for probabilities. *arXiv preprint arXiv:2107.09148*, 2021.

- [18] Steven L Heston. A closed-form solution for options with stochastic volatility with applications to bond and currency options. *The review of financial studies*, 6(2):327–343, 1993.
- [19] Christian Kahl and Peter Jäckel. Fast strong approximation Monte Carlo schemes for stochastic volatility models. *Quantitative Finance*, 6(6):513–536, 2006.
- [20] Sebastian Krumscheid and Fabio Nobile. Multilevel Monte Carlo approximation of functions. *SIAM/ASA Journal on Uncertainty Quantification*, 6(3):1256–1293, 2018.
- [21] Roger Lord, Remmert Koekoek, and Dick Van Dijk. A comparison of biased simulation schemes for stochastic volatility models. *Quantitative Finance*, 10(2):177–194, 2010.
- [22] Andreas Rössler Michael B. Giles, Kristian Debrabant. Analysis of multilevel Monte Carlo path simulation using the Milstein discretisation. *Discrete & Continuous Dynamical Systems - B*, 24(8):3881–3903, 2019.